Luminescent Carbon Nanodots Doped with Gadolinium (III): Purification Criteria, Chemical and Biological Characterization of a New Dual Fluorescence/MR Imaging Agent

Lucia Cardo,* Lydia Martínez-Parra, Michele Cesco, Begoña M. Echeverría-Beistegui, Marta Martínez-Moro, Natalia Herrero-Álvarez, Marta-Beraza Cabrerizo, Susana Carregal-Romero, Pedro Ramos-Cabrer, Jesús Ruiz-Cabello, and Maurizio Prato*

Carbon Dots (CDs) are luminescent quasi-spherical nanoparticles, possessing water solubility, high biocompatibility, and tunable chemical and physical properties for a wide range of applications, including nanomedicine and theranostics. The evaluation of new purification criteria, useful to achieve more reliable CDs, free from the interference of artifacts, is currently an object of debate in the field. Here, new CDs doped with gadolinium (Gd (III)), named Gd@CNDs, are presented as multifunctional probes for Magnetic Resonance Imaging (MRI). This new system is a case of study, to evaluate and/or combine different purification strategies, as a crucial approach to generate CDs with a better performance. Indeed, these new amorphous Gd@CNDs display good homogeneity, and they are free from emissive side products. Gd@CNDs (7–10 nm) contain 7% of Gd (III) w/w, display suitable and stable longitudinal relaxivity (r_1) and with emissive behavior, therefore potentially useful for both MR and fluorescence imaging. They show good biocompatibility in both cellular and in vivo studies, cell permeability, and the ability to generate contrast in cellular pellets. Finally, MRI recording T_1-weighted images on mice after intravenous injection of Gd@CNDs, show signal enhancement in the liver, spleen, and kidney 30 min postinjection.

1. Introduction

Carbon dots (CDs) are low dimensional quasi-spherical particles, first observed as side products during the purification of carbon nanotubes.[1] CDs are characterized by distinctive luminescence features and offer high versatility when tuning of the chemical or physical properties is required. Strategies to obtain CDs are usually divided in two categories:[2] (i) the top-down synthesis, occurring by fragmentation of high-sized carbon materials (i.e., graphite) or other carbon-containing natural sources (i.e., plants, food, food waste, etc.) and (ii) the bottom-up approach, in which selected molecular precursors are employed for pyrolysis or solvothermal reactions, to achieve particle-like materials through carbonization processes. The suitability of one synthetic approach certainly depends on the final application of the material, although bottom-up reactions usually allow better tuning and optimization

L. Cardo, L. Martínez-Parra, M. Cesco, B. M. Echeverría-Beistegui,
M. Martínez-Moro, N. Herrero-Álvarez, M.-B. Cabrerizo,
S. Carregal-Romero, P. Ramos-Cabrer, J. Ruiz-Cabello, M. Prato
Center for Cooperative Research in Biomaterials (CIC biomaGUNE)
Basque Research and Technology Alliance (BRTA)
Paseo de Miramón 194, Donostia-San Sebastián 20014, Spain
E-mail: lcardo@cicbiomagune.es; prato@units.it
L. Martínez-Parra, M. Cesco
University of the Basque Country UPV-EHU
Donostia-San Sebastián 20018, Spain

The ORCID identification number(s) for the author(s) of this article can be found under https://doi.org/10.1002/smll.202206442.

S. Carregal-Romero, P. Ramos-Cabrer, J. Ruiz-Cabello, M. Prato
Ikerbasque
Basque Foundation for Science
Bilbao 48013, Spain
S. Carregal-Romero, J. Ruiz-Cabello
CIBER de Enfermedades Respiratorias (CIBERES)
Madrid 28029, Spain
J. Ruiz-Cabello
Departamento de Química en Ciencias Farmacéuticas
Universidad Complutense de Madrid
Madrid 28040, Spain
M. Prato
Dipartimento di Scienze Chimiche e Farmaceutiche
Università degli Studi di Trieste
Trieste 34127, Italy

of the properties of CDs, such as chemical composition, luminescence features, surface charge, etc. In the last decade, extensive research has been dedicated to these materials; however, focusing most of the efforts on designing new families of CDs and exploring their potential in many fields, from nanomedicine to sensing, from catalysis to energy conversion.[3] Most recent debates highlight that greatest attention should now be given to improve purification strategies and structural understanding of CDs.[4] For example, a few works show that luminescence properties of well-known CDs (i.e., obtained by using citric acid and/or urea as precursors) are strongly affected by artifacts related to the presence of molecular side impurities.[5,6] Low cut-off dialysis is still the main (and often the only) strategy employed to isolate CDs after synthesis. However, it is now clearly emerging that this is not sufficient for many CDs preparations and a combination of alternative purification techniques (i.e., gel electrophoresis and chromatography) should be employed more routinely.[7–10]

Here, we aim at employing the technology of CDs to develop new multifunctional materials as contrast agents (CAs) in magnetic resonance imaging (MRI). As well known, most of CAs currently used in MR medical imaging, are gadolinium (III) (Gd) based complexes (Gadolinium-based Contrast Agents, GDCAs), whilst alternative systems, such as iron oxide and manganese compounds are still to be confirmed for a wide use in clinics.[11] Because of the electronic configuration of Gd (half-filled f7 shell), GDCAs are still the dominating paramagnetic CAs in clinics, providing ideal relaxivity properties, therefore the best "positive" contrast for MR enhancement. However, several concerns about their safety have arisen during the last decade,[12] often related to the possibility of free Gd released from the complex. Therefore, novel GDCAs should: (i) keep (or improve) the good relaxivity properties of currently employed CAs and (ii) own improved biosafety and biodistribution profiles, keeping suitable circulation times. Recent works have shown how nanotechnology could assist the design of new GDCAs possessing the above features and, at the same time, able to work as multifunctional platforms with extended detection modes, drug encapsulation, and biotargeting properties.[13,14]

CDs made by bottom-up approach, have proved to be highly suitable for this type of bioapplications: they are inherently luminescent, with tunable emission properties, and selected metal ions can be stably incorporated during CD assembly by solvothermal reactions. This leads to a potential dual (emission and MR) imaging system. In addition, depending on selected precursors, CDs present reactive groups (i.e., amino and/or carboxyl), typically useful for postsynthetic anchoring of biologically active molecules (i.e., drugs, targeting units). Last, but not least important, CDs are well known for their improved biocompatibility, high water solubility, and low or absent toxicity in vivo, and their usual size (below 10 nm) is ideal for the time scale of MRI scans, before kidney excretion.[15]

Herein we describe the preparation, purification, and characterization of amorphous carbon nanodots (CNDs), doped with Gd (Gd@CNDs), highlighting that additional purification steps are essential to achieve artifact-free and homogeneous materials. Gd@CNDs display stable relaxivity values that are comparable with commercially employed CA. They penetrate cells with remarkably low effect on cell viability and prove to be safe in preliminary 24 h in vivo experiments. Most importantly, they exhibit good contrast activity during MRI scanning in cell pellets and mice.

2. Results and Discussion

2.1. Synthesis and Purification Strategies

Some recent examples of CDs doped with Gd (III) have been reported. However only a small number of systems have been screened in vivo.[16–22] Very recently, Zheng and co-workers developed a graphitic Gd-CDs system conjugated with an aptamer for tumor targeting, observing the material accumulated in the tumor area both by MRI and by in vivo fluorescence imaging.[22] Few other examples of Gd-CD systems tested in vivo also employ conjugation with targeting units, which promote the accumulation of the material at one defined biological target and, consequently, an enhanced contrast activity. This is a very valid approach in theranostic, but systems able to generate contrast during targeting-free biodistribution experiments are also required. This is even more rarely reported when employing CDs as nanoscaffold,[16,21] because the design of agents with the right combination of pharmacokinetics and contrast enhancement properties, is highly challenging.

Here, we employed β-alanine (β-Ala), ethylenediaminetetraacetic acid (EDTA) and GdCl₃ as new set of precursors for the microwave-assisted hydrothermal reaction (**Scheme 1**).

We and others[23,24] have reported that amino acids are very suitable precursors to generate CDs, because they are (i)
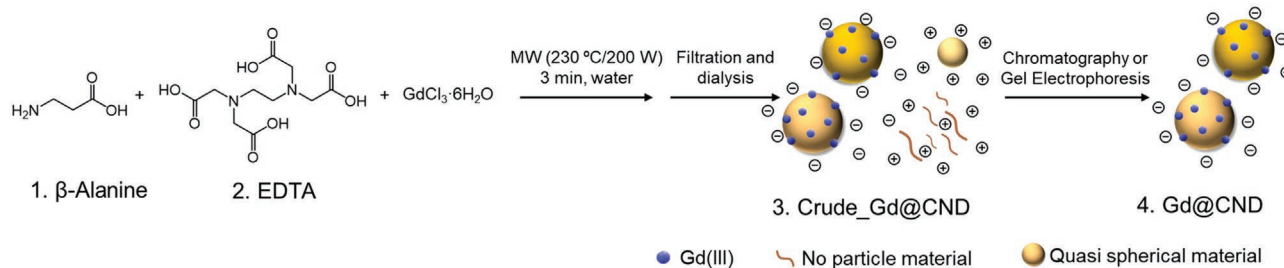
Scheme 1. Synthesis of gadolinium-doped Carbon Nanodots (CNDs). Compound 3, crude_Gd@CND, is obtained after filtration and dialysis and include CNDs doped with Gd (III) mixed with positive particle-like materials and other larger polymeric like aggregates. Compound 4, Gd@CND is the pure formulation obtained after gel electrophoresis or chromatography, including negatively charged, Gd doped, quasi-spherical CNDs only.
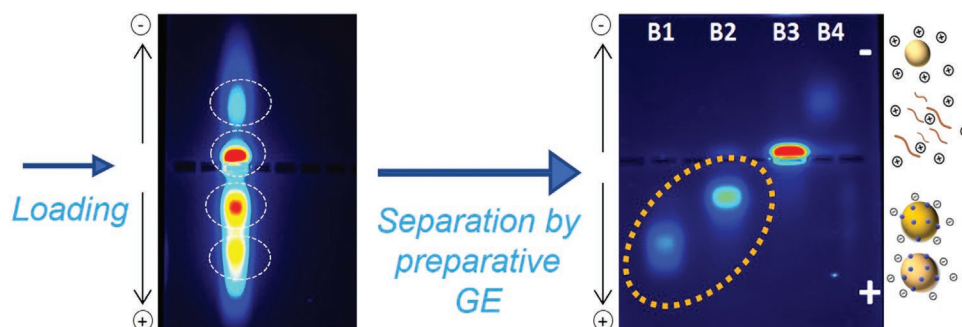
Figure 1. On the left, gel electrophoresis (GE, 1% agarose in 1× TAE buffer) of crude_Gd@CND (after dialysis and freeze drying) showing 4 populations of material (highlighted with dashed circle). Samples were loaded in the middle of the gel. The 4 compounds were isolated by preparative GE (see Figure S1 in the Supporting Information) and again analyzed to confirm separation (on the right); B1 and B2 (highlighted with dashed lines on the right) contain 2% and 4% w/w of gadolinium respectively (by ICP-MS).

naturally occurring (therefore facilitating biocompatibility of the final material) and (ii) a source of nitrogen, which is known to improve QY in luminescent CDs. EDTA is the chelating component that should assist the stable incorporation of gadolinium within the particle. The reaction was performed in water using a CEM Discover-SP microwave, for 3 min at 230 °C, followed by filtration (2 μm), 72 h dialysis (MWCO 500–1000 Da) against water and freeze drying. This yielded a light brown water-soluble powder named as **crude_Gd@CND**, containing 13% of gadolinium, by ICP-MS analysis.

Dialysis is typically the final purification step of all Gd-CDs systems reported so far (to the best of our knowledge). However here we observed that this was not sufficient to achieve an acceptable homogenous system. We employed agarose gel electrophoresis (GE) to analyze the composition of crude_Gd@CND. By loading the material in the middle of the gel, we observed the presence of at least four populations of material (indicated as **B1**, **B2**, **B3**, and **B4_Gd@CND** in **Figure 1**), of which two are positively charged and two are negatively charged. We optimized a versatile protocol to perform GE on a preparative scale, as purification tool to achieve the separation of the four components of the mix in crude_Gd@CND. Briefly, larger agarose gels were prepared (150 × 100 mm) and the crude compound (up to 10 mg) was loaded using a 1 mL capacity well (110 × 1.5 mm, well size). The four bands were excised from the gel and the purified material was extracted by "freeze and spin" method (see more details in Experimental Section and Figure S1 in the Supporting Information), followed by further characterization. As first important finding, only isolated B1 and B2 contain Gd (III), 2% and 4% by ICP-MS analysis respectively, whilst gadolinium was absent in the positive compounds B3 and B4. Optical spectroscopy characterization showed that all 4 compounds own similar UV–vis profiles (**Figure 2**A). They also show similar emission profiles, all depending on the excitation wavelength (λ_{ex}), a known feature of amorphous carbon dots.[4] However, using lower λ_{ex} (i.e., 320, 350 nm) the emission bands are in some cases shifted up to 18 nm indicating structural differences (Figure 2; Figure S2, Supporting Information).

Atomic force microscopy (AFM) analysis of crude_Gd@CND shows presence of particles (4–12 nm) together with larger particles or aggregates and other materials with no specific shape; instead, AFM images of B1, B2, and B4_Gd@CND consists of particles with narrower size distribution (5–12 nm), whilst larger

materials are mainly present in B3 (**Figure 3**A,B; Figure S3, Supporting Information). Transmission electron microscopy (TEM) analysis is usually challenging for amorphous CNDs, because the high content of carbon, the lack of defined morphology and their small size drastically reduce their contrast in TEM images. Indeed, TEM analysis of crude_Gd@CND only revealed the presence of very large impurities which possibly mask the presence of smaller particles. Nevertheless, isolated B1 and B2_Gd@CND are reasonably detectable in TEM, with a size distribution comparable with that measured by AFM (Figure 3C,D; Figure S4, Supporting Information).

Taken together, the standard hydrothermal procedure described above, followed by only dialysis, yielded negatively charged CDs doped with Gd (III) (B1 and B2). However, these particles are mixed with positively charged side products either particle-like, material behaving like amorphous CDs (B4), or material of larger size and undefined shape (in B3). Importantly, all the components of the mix display excitation-dependent fluorescence, with similar intensities, meaning that this desired luminescent property could derive either from gadolinium-doped CDs or from unwanted side impurities. Herein, we aimed to obtain fluorescent and stable Gd-doped CNDs, therefore we did not further characterize B3 and B4_Gd@CND, but we rather focused on exploring purification methods to isolate Gd-CNDs with suitable homogeneity and free from fluorescent artifacts.

The preparative GE procedure described above and in Figure S1 (Supporting Information), proved to be a valid method in our hands to separate the compounds of interest. However, this procedure presents a few intrinsic drawbacks, generally related to this specific separation method: the loading capability in GE is relatively low (up to 8–10 mg for each standard preparative set-up, commonly found in research laboratories) and the extraction of the material from the excised agarose bands requires more expensive and time-consuming procedures (see Experimental Section and additional observation in Figure S1 in the Supporting Information). Therefore, we explored alternative chromatography-based methods. Size exclusion chromatography (SEC) has been reported as a method to analyze or purify CDs, and here we used an Ultrahydrogel 120 Column from Waters connected to a High-Performance Liquid Chromatography system (HPLC). We explored several conditions (buffers, pH, and flow rate, see Figure S5 in the Supporting Information),
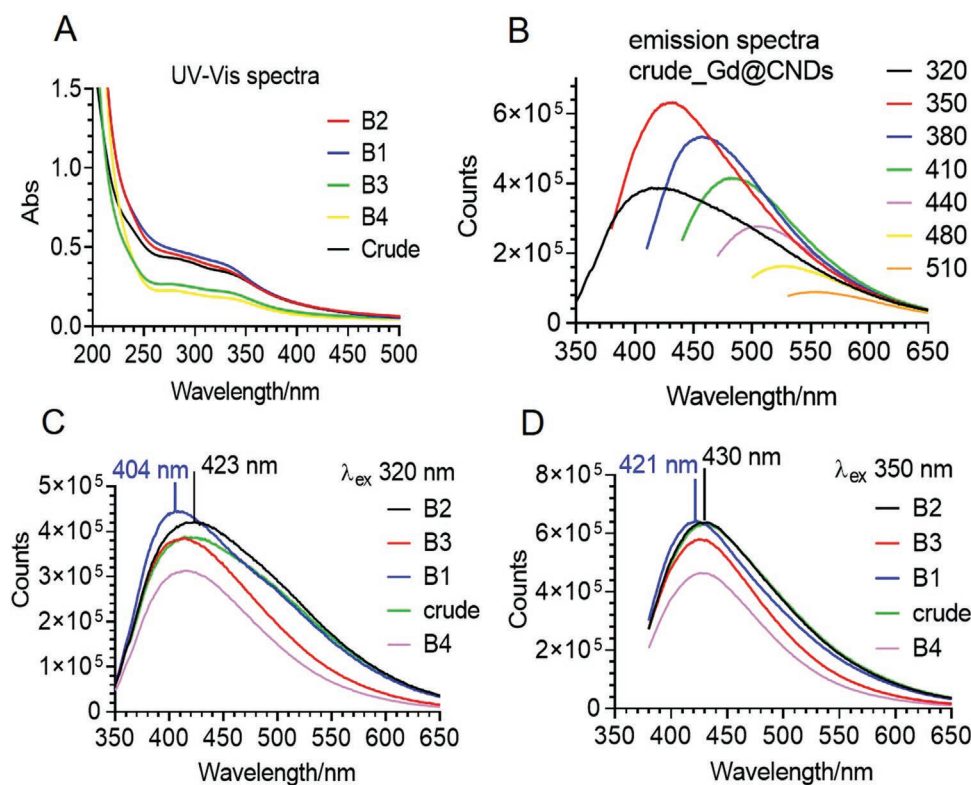
Figure 2. A) UV–vis spectra of crude_Gd@CND compared with the 4 compounds separated by GE (Figure 1, right). B) Emission spectra of crude_Gd@CND at different excitation wavelengths (λ_{ex} in the legend). Emission spectra of separated B1, B2, B3, and B4_Gd@CND are in Figure S2 in the Supporting Information; C,D) emission spectra of the 5 compounds (100×10^{-6} M of crude, B1, B2, B3, and B4) at λ_{ex} of 320 and 350 nm respectively.
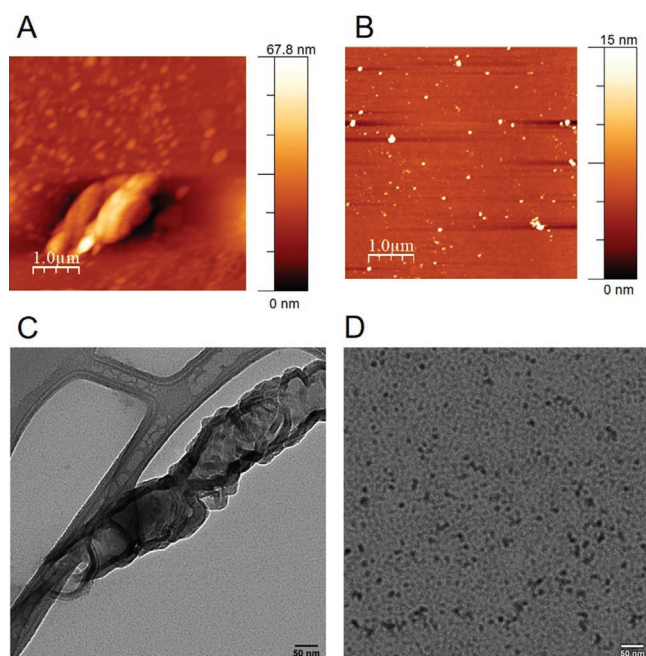

Figure 3. AFM images of A) crude_Gd@CND and B) B1_Gd@CND (isolated by GE); TEM images of C) crude_Gd@CND and D) B1_Gd@CND (scale bar 50 nm). See additional data in Figures S3 and S4 in the Supporting Information.

but we did not achieve a satisfactorily resolved chromatogram or a profile that would improve times and yields, compared to the purification by GE. Although SEC was not the best option in this case, we further confirmed that our synthesized crude contains emissive materials with very similar sizes, suggesting that, in general, SEC-based methods must be evaluated carefully for the purification of CDs.

Removal of B3 and B4_Gd@CND from the mix was essential, because they would eventually disturb as emissive artifacts. However, we reasoned that the separation between B1 and B2 was not truly needed. In fact, they both contain Gd (III) from ICP-MS and XPS analysis. Gd content in B2 was slightly higher (4% w/w vs 2% by ICP-MS), consistent with the slower electrophoretic mobility when compared to B1. Significant differences in size and shape were not observed by TEM and AFM (Figures S3 and S4, Supporting Information). Finally, and most importantly, we ran both relaxivity measurements and key cell biology studies using B1 and B2_Gd@CND separately and we did not observe any meaningful difference between the two materials (see sections below and Figures S11 and S13 in the Supporting Information). Convinced that no valuable advantage could come from separating these two components, we aimed to obtain B1 and B2 combined in one final and optimized formulation. For this reason, we selected ion exchange chromatography (IEC) as the method able to separate the components of crude_Gd@CND by charge. Also in this case, we evaluated different protocols, as the material showed different affinity with
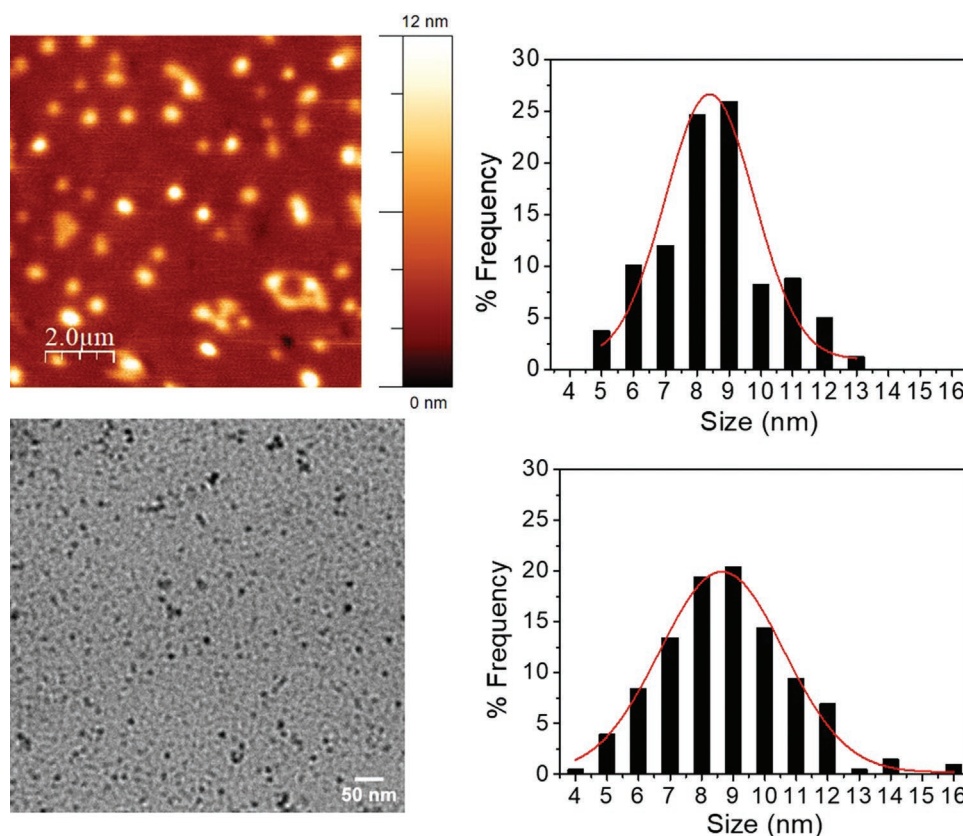
Figure 4. AFM (top) and TEM (bottom) images of Gd@CND (isolated by ion exchange) with corresponding size distributions (% of frequency of each size particle).

the stationary phase/eluent combinations tested (see Figure S6 in the Supporting Information). The pre-packed anion weak exchange SPE (solid phase extraction) column, from Phenomenex, was the selected system able to separate efficiently the negatively charged final material (named Gd@CND, compound 4 in Scheme 1), from the unwanted positively charged emissive products.

TEM and AFM analyses confirmed the amorphous morphology of Gd@CND, and the size distribution measured with these two techniques is highly comparable: ≈70% of detected quasi-particles display longitudinal size between 7 and 10 nm (**Figure 4**). ICP-MS analysis reveal 7% w/w of gadolinium: the loss of gadolinium, compared to crude_ Gd@CND was always observed after any purification procedure (GE, SEC, or IEC). Probably, this occurs because weakly coordinated metal ions are removed from the system, supporting the importance of purification to achieve a system with higher stability. The negative charge observed by GE is possibly due to the presence of carboxylic groups, introduced through both EDTA and β-Ala employed as precursors. We evaluated this more in detail employing the Gran Plot analysis method (Figure S10, Supporting Information),[25,26] measuring a pK_a of 2.9 and estimating the material carrying 21 500 µmol g^{-1} acidic sites.

X-ray photoelectron spectroscopy (XPS) was used to analyze the coordination environment of the metal. The survey spectrum reveals the following elements (in atomic percentage): 72.7% Carbon, 16.6% Oxygen, 9.8% Nitrogen, and 0.8%

Gadolinium (**Figure 5**A). By converting these data to mass percentage, also this technique confirms 8% of Gd w/w, well consistent with the amount of metal found by ICP-MS. The typical Gd 4d profile appears as two peaks at 143.5 eV, 148.1, adjacent to the peak at 154 eV related to Si 2s (Figure 5B). This last is knowingly originating from the glass of the gold support employed for the measurement, but its contribution was included for the fitting process of Gd 4d.[27] Deconvolution of the signal reveals the components at 141.2, 142.2, 143.2, and 148.1 eV, assigned to the presence of Gd_2O_3, whilst the components at 144.2 and 145.2 eV suggest $Gd_2(C_2O_4)_3$ environment type. This is consistent with the components observed upon deconvolution of Oxygen 1s signal (Figure 5D), at 531.1 and 532.6 eV, possibly corresponding to Gd_2O_3 and $Gd_2(C_2O_4)_3$ respectively. Carbon 1s signal at 285.4 eV include four components with following binding energies and bond designations (Figure 5C): 284.8 eV (C–C/C=C bonds), 285.8 eV (C–O bond), 287.3 (O–C–O bonds), and 288.1 (O–C=O bonds) eV, being the last three consistent with presence of carboxylic groups. Finally, Nitrogen 1s spectrum shows two components at 399.5 and 400.6 eV, which are attributed to the pyridinic C=N bond and pyrrole C–N bond, respectively, usually expected in CDs as a result of carbonization processes (Figure 5E).

Additional characterization techniques were employed to evaluate the homogeneity of the system and to confirm the absence of starting materials and/or molecular side products. 1H NMR spectrum of Gd@CND, shows broad signals,
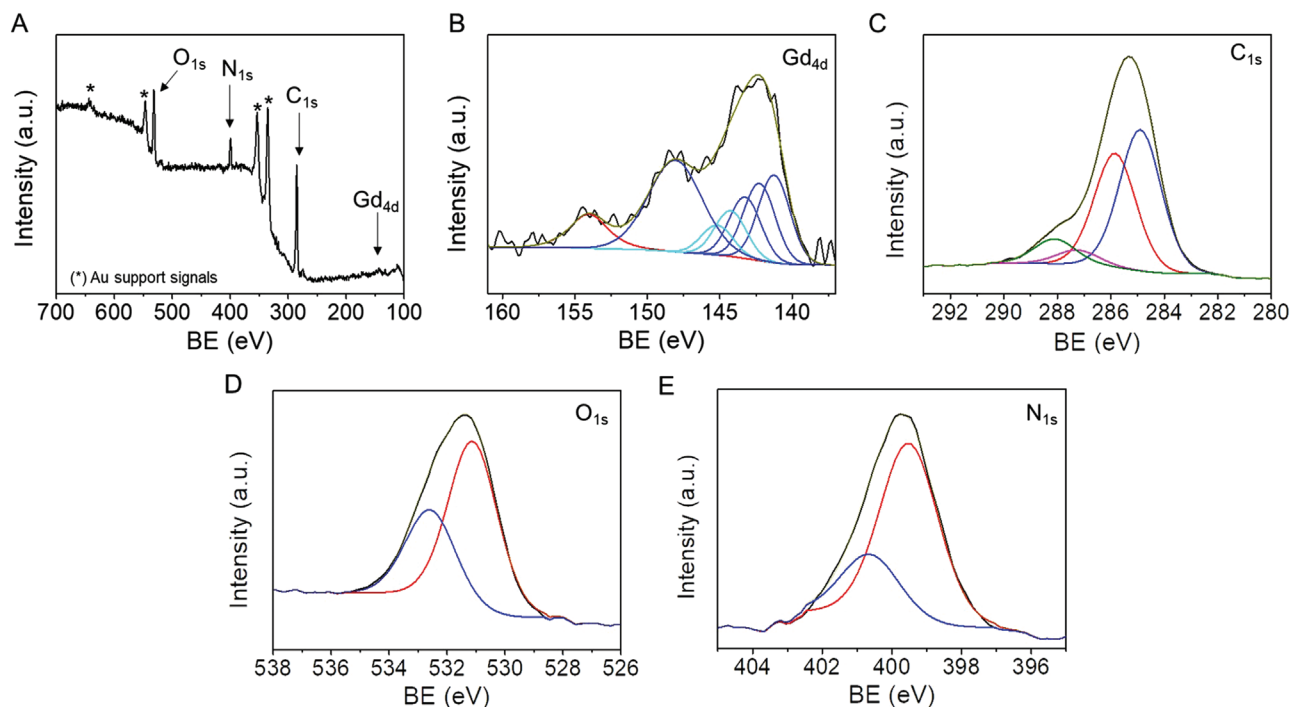
**ADVANCED
SCIENCE NEWS**

www.advancedsciencenews.com

NANO · MICRO

small

www.small-journal.com

Figure 5. XPS spectra of Gd@CND: A) survey showing all the elements present during the analysis (* are signals corresponding to Au, from the support employed). Deconvolution and curve-fitting of B) Gd 4d, C) C 1s, D) O 1s, and E) N 1s signals.

as expected for CNDs,[6] confirming the carbogenic nature of the material and the absence of starting materials (Figure S7, Supporting Information). Most importantly, diffusion ordered spectroscopy (DOSY) analysis shows that this system has one distinctive diffusion coefficient, smaller than the coefficient of a molecule such as the starting β-Ala (**Figure 6**; Figure S8, Supporting Information).[28] This confirms that Gd@CNDs behave as a homogeneous nanomaterial and, at the same time, side products of lower molecular weight were not observed.

Finally, thermogravimetric analysis (TGA) was performed to estimate the thermostability of our nanomaterial. **Figure 7** shows the decomposition profile (under inert atmosphere) of Gd@CNDs together with its starting precursors and crude_Gd@CNDs, for comparison. The multi-step low mass decrease

(20%) of $GdCl_3 \cdot 6H2O$ is consistent with the formation of gadolinium oxide species.[29,30] Gd@CNDs mass loss occurs through two main large stages, between 120 and 310 °C (with a possible overlapped shoulder at 250 °C) and between 320 and 500 °C. Furthermore, the thermogram shows a mass decrease of 55% only, possibly due to (i) the presence of residual gadolinium oxide species, well consistent with the control (the salt alone) and the XPS analysis above, or (ii) the existence of a highly stable carbonized component (known for carbon-based materials) or, most likely (iii) a combination of these two factors. In comparison, starting materials, EDTA[31] and β-Ala, degrade completely through rapid weight drop stages (typical of small organic molecules). Crude_Gd@CNDs also shows incomplete weight loss through at least 4 stages, as expected for
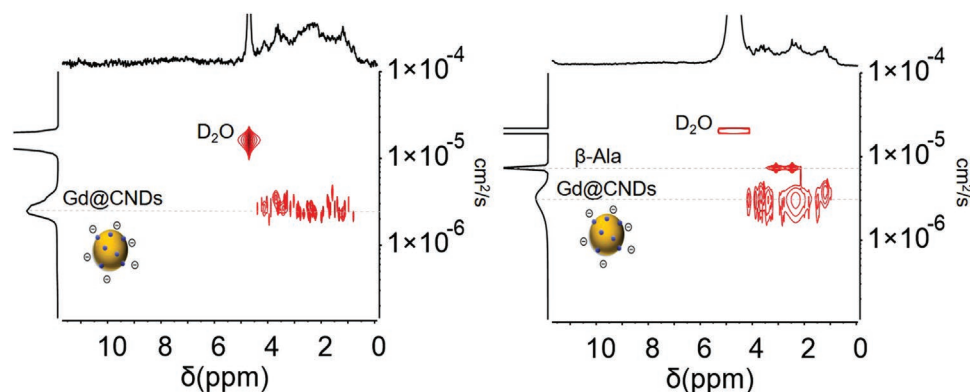

Figure 6. DOSY spectrum (D_2O, 500 MHz) of Gd@CNDs (left) and Gd@CNDs mixed with β-Ala as a reference (right). The amino acid, being a small molecule, has a higher diffusion coefficient compared to the Gd@CNDs system.

ADVANCED
SCIENCE NEWS
www.advancedsciencenews.com

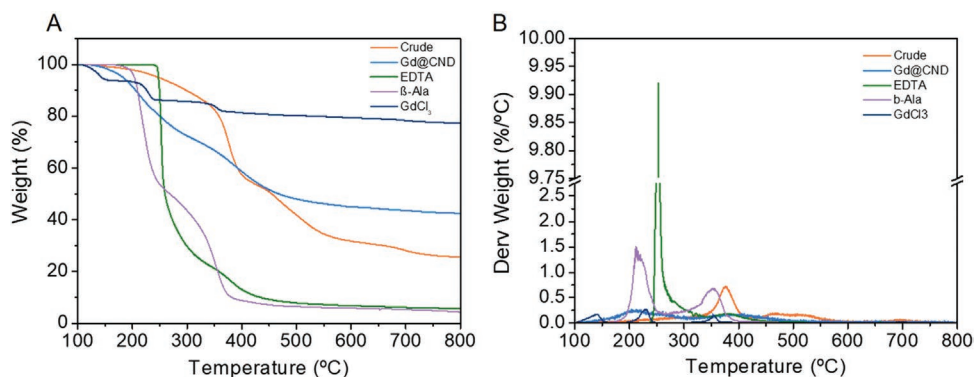NANO · MICRO
small
www.small-journal.com

Figure 7. A) TGA thermograms and B) related derivative curves of Gd@CND compared with precursors and crude_Gd@CND under inert atmosphere.

a more complex mixture. Also, it is known that degradation of nanomaterials in TGA starts from surface groups; in fact, Gd@CNDs and crude_Gd@CNDs show a different degradation profile between 150 and 400 °C, probably because the crude material is a mix of positively and negatively charged components, as observed by GE (Figure 1). Finally, crude_Gd@CNDs displays a higher, yet not complete, weight loss (75%), consistent with the possible presence of materials of polymeric nature in the crude, as discussed above, which are not stable during TGA. Therefore, also this analysis suggests that standard dialysis procedures cannot eliminate large no-carbonaceous side-products eventually formed during microwave-assisted reactions.

2.2. Relaxivity and Stability

Gd(III) based compounds are employed as T_1 contrast agents, providing a bright signal when they accumulate in tissues. To

evaluate the performance of Gd@CND as contrast enhancing agents in MRI, longitudinal and transversal relaxation rates were measured at different concentrations of material and using two different magnetic fields (1.5 and 7 T, **Figure 8**).

The resulting longitudinal relaxivity values (r_1), calculated from the slope of the linear trend, are comparable and even higher than several commercial GBCAs (i.e., Gadavist, 5.2 × 10^{-3} M^{-1} s^{-1})[32] as well as other single nanoparticulate systems already reported. Ding et al., for example, recently discussed the magnetic properties of nanomaterials like RGD-Gd@C-dots, Gd-CQDs, Gd@GCNs, Gd-CDs, Folate-GdGCDs, etc., (see, Table 2 from Ref. [33]), all displaying r_1 values comparable with our system. On the other hand, nanomaterials based on larger supramolecular complexes, like the Gd-doped graphene quantum dots and other systems, also discussed by Ding et. al., own higher relaxivity values. Possibly, these sorts of materials take advantage of their volume and specific area to profit from their inherent slower rotational correlation times, resulting on
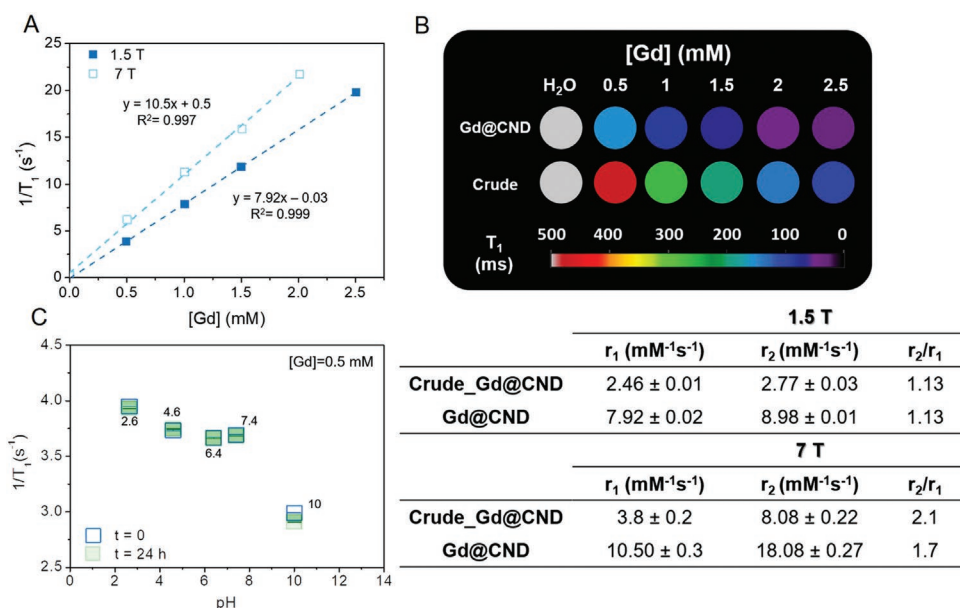

Figure 8. A) Longitudinal relaxation rates ($1/T_1$) as a function of Gd concentrations (dash line: lineal fitting) of Gd@CND, at 1.5 and 7 T (at 37 °C). B) T_1 maps MR images of CNDs phantoms at 7 T, comparing Gd@CND before and after purification (*Water values are saturated in the image due to scale). Relaxivity values are summarized in the bottom right table. C) Longitudinal relaxation rate of Gd@CND (0.5 × 10^{-3} M of Gd) at different pH, measured at time 0 and 24 h.

	1.5 T		
	r_1 (mM^{-1}s^{-1})	r_2 (mM^{-1}s^{-1})	r_2/r_1
Crude_Gd@CND	2.46 ± 0.01	2.77 ± 0.03	1.13
Gd@CND	7.92 ± 0.02	8.98 ± 0.01	1.13
	7 T		
	r_1 (mM^{-1}s^{-1})	r_2 (mM^{-1}s^{-1})	r_2/r_1
Crude_Gd@CND	3.8 ± 0.2	8.08 ± 0.22	2.1
Gd@CND	10.50 ± 0.3	18.08 ± 0.27	1.7

ADVANCED
SCIENCE NEWS
www.advancedsciencenews.com

NANO · MICRO
small
www.small-journal.com

improved relaxivity properties, when compared to single particle-like materials like ours. Therefore, the level of Gd-doping into our CD system, seems adequate to achieve a promising low dimensional contrast nanomaterial. Furthermore, the low ratio r_2/r_1, below 3 at both 1.5 and 7T, validated them as T_1 or positive contrast agents.[34] We also evaluated relaxivity values of crude_Gd@CND (Figure 8B), and B1 and B2_ Gd@CND separately (Figure S11, Supporting Information). In the latter cases, r_1 values of the two compounds were comparable (4.6 and 3.8×10^{-3} $\text{M}^{-1}\text{s}^{-1}$, for B1 and B2 respectively, at 1.5 T). This, together with the morphological analysis described above, was a further motivation for combining them in one formulation (Gd@CND) with a better performance. On the other hand, r_1 values of crude_Gd@CND are approximately threefolds lower, compared to the purified Gd@CND, suggesting that the high content of side products affects this fundamental property of the material.

As a proof of stability of Gd@CND, we measured relaxivity in water at different time points for 72 h, observing no changes (Figure S12, Supporting Information).[35] We also measured relaxivity at different pH (Figure 8C): minor differences were observed in the pH range between 2.6 and 7.4, and a 1.4 folds decrease of r_1 at pH 10. However, all the values were kept con-

stant in time (measured after 24 h), suggesting that the contrast activity of gadolinium in the system is time constant. Therefore, the system is highly stable, but r_1 values slightly depend on the pH of the system, confirming that carboxylic groups are involved in the interaction with the metal.

2.3. In Vitro Studies and In Vivo Imaging of Gd@CND

CDs are highly attractive for medical applications because of their excellent biocompatibility and biosafety. To confirm that Gd@CNDs retain this essential feature, we performed preliminary cell viability studies using a widely employed lung cancer cell line, A549 (**Figure 9**A). Despite treatment of cells with high concentration of material (up to 1000 µg mL^{-1}), no significative cytotoxicity was observed during 24 h incubation. Complete loss of cell viability was observed only at 72 h incubation time and at rather high concentrations (IC50 (72 h) 285 µg mL^{-1}), and this is usually considered as minor cytotoxicity.[36] We were able to observe the material into cells by confocal laser scanning microscopy, CLSM (Figure 9B), implying that the blue emission of the material could be employed as a second imaging mode in a biological environment.
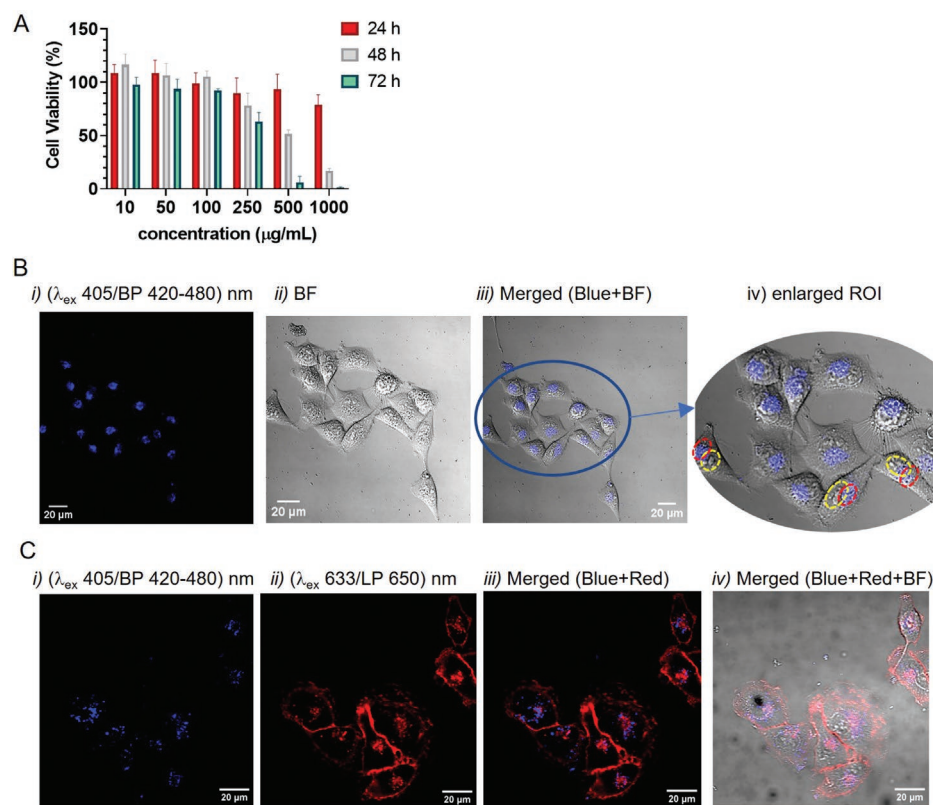

Figure 9. A) Viability of A549 cell line by MTT assay: percentage (%) of viability in cells treated with increasing concentrations of Gd@CNDs and using different incubation times (24, 48, 72 h); % is in respect to control (untreated cells, 100% cell viability; data are the mean ± SD of 3 independent experiments, each repeated with triplicates (*n* = 3)). B) CLSM images (20× air) of live A549 cells treated with 100 µg mL^{-1} of Gd@CNDs for 24 h; from left to right: (i) blue emission, (ii) bright field (BF), (iii) merged images of blue+BF, and (iv) the enlargement of a ROI highlighting the nucleus region and CDs accumulation area (yellow and red dashed respectively). C) CLSM (63× oil) of live A549 cells treated with 100 µg mL^{-1} of Gd@CNDs for 24 h followed by cellular membrane staining with CellMask Deep Red; left to right: (i) blue emission, (ii) red emission, (iii) merged images of blue+red and (iv) merged images blu+red+BF. Each image report scale and excitation wavelengths (λ_{ex})/filters employed (additional images and z-stack experiment in Figure S14 in the Supporting Information).

**ADVANCED
SCIENCE NEWS**

www.advancedsciencenews.com

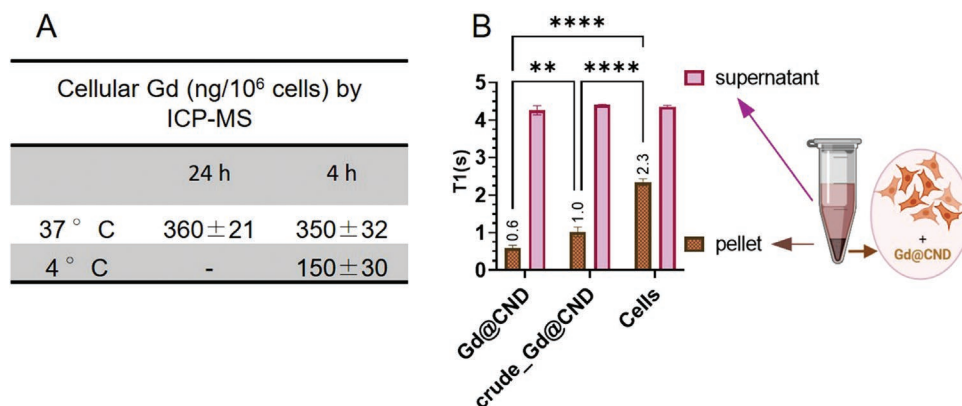**NANO · MICRO
small**

www.small-journal.com

Figure 10. A) Gadolinium (in ng per million of cells) measured from digested cellular pellets (A549) by ICP-MS analysis, upon treating cells with 100 µg mL^{-1} of Gd@CNDs at different temperatures and incubation times. B) Measured proton T_1 (s) of cell pellets previously treated with 100 µg mL^{-1} of Gd@CNDs for 24 h, compared with T_1 of untreated cell pellets and T_1 of supernatant (cell medium) to ensure that the observed decrease of T_1 is related to the pellets only and that Gd leakage is not involved. In both (A) and (B), results are the mean±SD of 3 independent experiments, each performed in duplicate; in (B) ** is $P \leq 0.01$ and **** is $P \leq 0.0001$.

By comparing fluorescence and bright field images, the material seems to have accumulated in the cytosol region and not involved with the nucleus area. Furthermore, cells, previously incubated with Gd@CNDs for 24 h, were treated with a red emissive marker for cellular membrane (CellMask Deep Red (Invitrogen)). Qualitatively, CDs (blue signal in Figure 9C) poorly overlap with the red marked cellular membrane; also quantitative analysis confirms a rather low percentage of red/blue colocalization (9.4%, see Figure S14 in the Supporting Information). All this supports the possibility that Gd@CNDs penetrate cells and accumulate in the cytosol region. By ICP-MS analysis, we analyzed the amount of gadolinium associated to cells, after 4 and 24 h incubation. In both cases we estimated similar values, around 350 ng of Gd per million cells (ng/10^6 cells), generally in line with the uptake of metal-based agents into cells (**Figure 10**A). The possibility of an energy-dependent cellular uptake of Gd@CND was evaluated by incubating cells with the material at 4 and 37 °C followed by measuring the amount of Gd associated to cells by ICP-MS. The results, summarized in Figure 10A, indicate that: (i) at 37 °C, the same amount of Gd was incorporated into cells after 4 or 24 h, suggesting a rather fast cellular uptake; (ii) the incubation at 4 °C caused a remarkable decrease of Gd cellular assimilation (about 58%); this eventually occurs when energy is required for the cellular uptake process and suggests Gd@CND penetrate cells through endocytosis-based mechanisms.[37]

Finally, we measured proton T_1 relaxation in cell pellets upon cellular uptake of Gd@CNDs (Figure 10B): the experiment shows a remarkable decrease of cellular T_1 ($\approx$75%) due to the presence of the material. Also in this case, the effect is reduced by using crude_Gd@CNDs, whilst separated B1 and B2_Gd@CNDs behave as Gd@CNDs (Figure S13, Supporting Information). All this indicates that the material is cell-permeable, probably by endocytosis-based mechanisms; it is found accumulated in the cytosol region and is able to actively work as contrast agent and luminescent probe in a cellular environment. In general, cell permeability widens the range of applications in the field of new GDCAs, as most

of the agents employed in clinic, work outside cells. For this reason, highly detailed cellular studies are ongoing, to understand the preferred endocytosis mechanism employed, possible targets in the cytosol, cellular escape, and long-term cytotoxicity.

Finally, we performed first biodistribution studies of Gd@CNDs in vivo. C57BL/6JRj female mice ($n = 3$) were imaged before administration of CDs to acquire reference scans. Then, 100 µL of Gd@CNDs (containing 0.1 mmol Gd/kg) or PBS (control) were injected into the mice through the tail vein. MR images of the abdomen were acquired using a T_1-weighted sequence at a series of time points (1, 2, and 24 h). T_1 maps and the decrease of T_1 values (in Concentration of Gd (*ng/millions of cells), measured by ICP-MS, from digested cell pellets, upon treating A549 cells with 100 µg mL^{-1} of Gd@CND, at 37 °C (for 4 and 24 h) and at 4 °C (for 4 h). Results are the average of three independent experiments ±SD. **Figure 11** and Figure S15 (Supporting Information) show Gd@CNDs accumulated after 1–2 h postinjection in liver, spleen and kidneys, indicating renal clearance. All T_1 values are mostly recovered within the first 24 h (Figure 10C). This is consistent with additional ex vivo experiments: mice were sacrificed after 24 h and the total residual gadolinium, detected in different organs (heart, liver, spleen, kidneys) was around 15% of the initial gadolinium administered (analyses performed by ICP-MS). The content of gadolinium was also measured in urine samples collected immediately after injection (time 0), after 1 and 24 h. Also in this case, $\approx$85% of the initial injected gadolinium was in the urine sample collected after 1 h (Figure S16, Supporting Information). According to literature,[36,37] this low percentage of residual gadolinium in only 24 h is very encouraging. Finally, no damage caused by Gd@CNDs was observed in histological analyses of different organs (Figure S17, Supporting Information). Overall, Gd@CNDs are able to generate an evident contrast enhancement in vivo, without the need of being accumulated to specific biotargets. They follow a clear hepatic and, mainly, renal elimination[38,39] occurring mostly during the first 1–2 h and almost complete in 24 h.
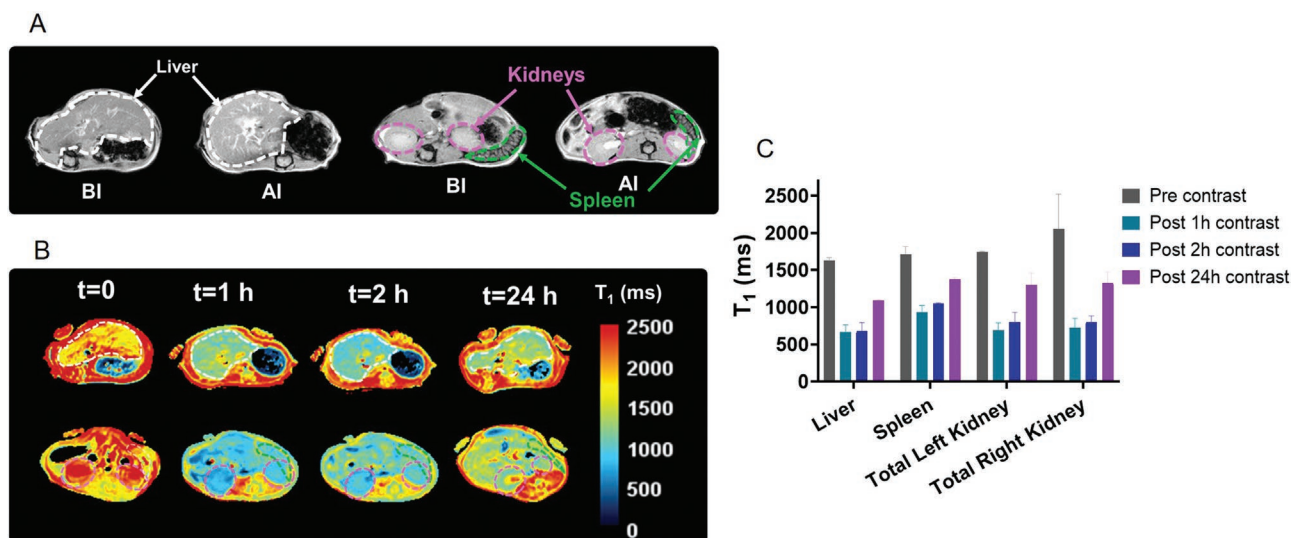
**ADVANCED
SCIENCE NEWS**

www.advancedsciencenews.com

**NANO · MICRO
small**

www.small-journal.com

Figure 11. A) Axial anatomical images of the abdomen of a mouse before (BI) and after (AI) intravenous injection of Gd@CND (a longitudinal image is in Figure S15 in the Supporting Information). B) T_1 relaxation maps showing mouse axial view at different time points post injections of Gd@CNDs. C) T_1 relaxation values for the analyzed organs prior to and after administration of the nanomaterial (n = 3, results are the mean±SD).

3. Conclusion

Carbon-based low-dimensional materials own a vast potential for different applications in nanomedicine, mainly because of their safety, stability, and high solubility in biological systems. Bottom-up approaches, using solvothermal reactions, are powerful tools to create large libraries of multifunctional carbon dots (CDs), but, at the same time, they might lead to material formulations with high heterogeneity (therefore with physical/chemical properties difficult to be controlled) and presence of artifacts able to affect their performance. This could be solved by exploring and intensifying the use of different purification methods in combination with or alternative to dialysis, which is still the main and too often sole method employed in the field of CDs engineering. Here, we aimed to achieve CDs doped with gadolinium (III) as multimodal nanomaterials for MRI. At the same time, we generated a clear case of study to highlight the importance of CDs purification, by combining different methods if necessary. In fact, purification based on dialysis only yielded a mixture of negatively charged Gd-doped CDs, positively charged undoped CDs and larger materials with undefined shape. All the components of the mix presented comparable emissive behavior, which is a major issue when luminescence of the material is one of the functions needed for imaging. Furthermore, the presence of side products compromised the characterization process and affected other key properties of the material, such as homogeneity and relaxivity (also in cellular systems). We explored (for the first time for Gd-CD systems) gel electrophoresis (GE), size exclusion chromatography (SEC) and ion exchange chromatography (IEC) as possible purification methods, and selected this last to obtain an optimized and homogenous final formulation, named Gd@CND. These new amorphous gadolinium-doped CDs are negatively charged, possibly due to the presence of carboxylic groups, containing 7–8% w/w of gadolinium (III), and 7–10 nm as main range (over 70%) of size distribution. They display dif-

ferent emissive profiles, depending on excitation wavelength, as expected for amorphous CDs. Relaxivity (r_1) values of Gd@CND, at 1.5 and 7 T, are comparable with commercial contrast agents and, importantly, are stable in time and at different pH conditions. In cellular studies, Gd@CNDs are cell permeable although they do not majorly affect cell viability. They are detected by confocal fluorescence microscopy in cells and they generate enhanced contrast in cellular pellet. More detailed cellular studies are currently ongoing, to elucidate their activity, targeting, and distribution in cellular environments. Finally, and most importantly, in vivo studies confirmed good biocompatibility of Gd@CNDs, with excretion via renal system in 24 h (which is ideal for contrast agents) and the ability to generate bright contrast (especially in the liver, spleen, and kidney) without the assistance of specific biological targeting (differently from most of the few Gd-CDs systems reported so far). Current experiments focus on finding strategies to functionalize these new CDs with biologically active moieties, especially drugs and biological markers. Thanks to their stability, good MRI performance in vivo (yet easy body excretion) and their potential availability for multifunctionalization, nanomaterials like Gd@CNDs are valuable for applications in theranostics, as potentially able to deliver and track therapies at the same time.

4. Experimental Section

An extensive Experimental Section can be found in the Supporting Information. All animal studies were performed at CICbiomaGUNE. Animals were maintained and handled following the Guidelines for Accommodation and Care of Animals (European Convention for the Protection of Vertebrate Animals Used for Experimental and Other Scientific Purposes). All animal procedures were performed under the European Union Animal Directive (2010/63/EU). Experimental procedures were approved by the local Ethical Committee of CIC biomaGUNE and by the local authorities (Diputación Foral de Guipúzcoa, project number PRO-AE-SS-091).

**ADVANCED
SCIENCE NEWS**

www.advancedsciencenews.com

NANO · MICRO

small

www.small-journal.com

Supporting Information

Acknowledgements

Conflict of Interest

The authors declare no conflict of interest.

Data Availability Statement

The data that support the findings of this study are available from the corresponding author upon reasonable request.

Keywords

[1] X. Xu, R. Ray, Y. Gu, H. J. Ploehn, L. Gearheart, K. Raker, W. A. Scrivens, *J. Am. Chem. Soc.* **2004**, *126*, 12736.

[2] L. Đorđević, F. Arcudi, M. Cacioppo, M. Prato, *Nat. Nanotechnol.* **2022**, *17*, 112.

[3] J. Liu, R. Li, B. Yang, *ACS Cent. Sci.* **2020**, *6*, 2179.

[4] G. Ragazzon, A. Cadranel, E. Ushakova, Y. C. Wang, D. M. Guldi, A. L. Rogach, N. A. Kotov, M. Prato, *Chem* **2021**, *7*, 606.

[5] J. B. Essner, J. A. Kist, L. Polo-Parada, G. A. Baker, *Chem. Mater.* **2018**, *30*, 1878.

[6] B. Bartolomei, A. Bogo, F. Amato, G. Ragazzon, M. Prato, *Angew. Chem., Int. Ed.* **2022**, *61*, e202200038.

[7] M. Righetto, F. Carraro, A. Privitera, G. Marafon, A. Moretto, C. Ferrante, *J. Phys. Chem. C* **2020**, *124*, 22314.

[8] L. Liu, Z. Xu, *Anal. Methods* **2019**, *11*, 760.

[9] M. Otten, M. Hildebrandt, R. Kühnemuth, M. Karg, *Langmuir* **2022**, *38*, 6148.

[10] V. Michaud, J. Pracht, F. Schilfarth, C. Damm, B. Platzer, P. Haines, C. Harreiß, D. M. Guldi, E. Spiecker, W. Peukert, *Nanoscale* **2021**, *13*, 13116.

[11] Y.-D. Xiao, R. Paudel, J. Liu, C. Ma, Z.-S. Zhang, S.-K. Zhou, *Int. J. Mol. Med.* **2016**, *38*, 1319.

[12] R. J. McDonald, D. Levine, J. Weinreb, E. Kanal, M. S. Davenport, J. H. Ellis, P. M. Jacobs, R. E. Lenkinski, K. R. Maravilla, M. R. Prince, H. A. Rowley, M. F. Tweedle, H. Y. Kressel, *Radiology* **2018**, *289*, 517.

[13] A. Fatima, M. W. Ahmad, A. K. A. al Saidi, A. Choudhury, Y. Chang, G. H. Lee, *Nanomaterials* **2021**, *11*, 2449.

[14] J. Wahsner, E. M. Gale, A. Rodríguez-Rodríguez, P. Caravan, *Chem. Rev.* **2019**, *119*, 957.

[15] A. Merbach, L. Helm, E. Tóth, *The Chemistry of Contrast Agents in Medical Magnetic Resonance Imaging, Second Edition*, John Wiley & Sons, Ltd, Chichester **2013**.

[16] F. Du, M. Zhang, A. Gong, Y. Tan, J. Miao, Y. Gong, S. Zou, L. Zhang, L. Zhang, C. Wu, M. Sun, H. Ju, *Biomaterials* **2017**, *121*, 109.

[17] X. He, Q. Luo, J. Zhang, P. Chen, H.-J. Wang, K. Luo, X.-Q. Yu, *Nanoscale* **2019**, *11*, 12973.

[18] C. Lee, X. Liu, W. Zhang, M. A. Duncan, F. Jiang, C. Kim, X. Yan, Y. Teng, H. Wang, W. Jiang, Z. Li, J. Xie, *Nanoscale* **2021**, *13*, 9252.

[19] H. Chen, Y. Qiu, D. Ding, H. Lin, W. Sun, G. D. Wang, W. Huang, W. Zhang, D. Lee, G. Liu, J. Xie, X. Chen, *Adv. Mater.* **2018**, *30*, 1802748.

[20] H. Liao, Z. Wang, S. Chen, H. Wu, X. Ma, M. Tan, *RSC Adv.* **2015**, *5*, 66575.

[21] D. Bouzas-Ramos, J. Cigales Canga, J. C. Mayo, R. M. Sainz, J. Ruiz Encinar, J. M. Costa-Fernandez, *Adv. Funct. Mater.* **2019**, *29*, 1903884.

[22] M. Jiao, Y. Wang, W. Wang, X. Zhou, J. Xu, Y. Xing, L. Chen, Y. Zhang, M. Chen, K. Xu, S. Zheng, *Chem. Eng. J.* **2022**, *440*, 135965.

[23] J. Jiang, Y. He, S. Li, H. Cui, *Chem. Commun.* **2012**, *48*, 9634.

[24] F. Arcudi, L. Dordevic, M. Prato, *Angew. Chem., Int. Ed.* **2016**, *55*, 2107.

[25] J. A. Boiani, *Chem. Educ.* **1986**, *63*, 724.

[26] G. Filippini, F. Amato, C. Rosso, G. Ragazzon, A. Vega-Peñaloza, X. Companyó, L. Dell'Amico, M. Bonchio, M. Prato, *Chem* **2020**, *6*, 3022.

[27] T. B. Thiede, M. Krasnopolski, A. P. Milanov, T. de Los Arcos, A. Ney, H. W. Becker, D. Rogalla, J. Winter, A. Devi, R. A. Fischer, *Chem* **2011**, *23*, 1430.

[28] S. Cailotto, E. Amadio, M. Facchin, M. Selva, E. Pontoglio, F. Rizzolio, P. Riello, G. Toffoli, A. Benedetti, A. Perosa, *ACS Med. Chem. Lett.* **2018**, *9*, 832.

[29] I. v. Korzun, I. D. Zakir'yanova, E. V. Nikolaeva, *Russ. Metall.* **2018**, *8*, 722.

[30] I. V. Korzun, E. V. Nikolaeva, I. D. Zakir'yanova, *J. Therm. Anal. Calorim.* **2021**, *144*, 1343.

[31] A. Narayanan, R. Dhamodharan, *Carbohydr. Polym.* **2015**, *134*, 337.

[32] M. Rohrer, H. Bauer, J. Mintorovitch, M. Requardt, H.-J. Weinmann, *Invest. Radiol.* **2005**, *40*, 715.

[33] H. Ding, D. Wang, A. Sadat, Z. Li, X. Hu, M. Xu, P. C. de Morais, B. Ge, S. Sun, J. Ge, Y. Chen, Y. Qian, C. Shen, X. Shi, X. Huang, R. Q. Zhang, H. Bi, *ACS Appl. Bio Mater.* **2021**, *4*, 2798.

[34] S. Caspani, R. Magalhães, J. P. Araújo, C. T. Sousa, *Materials* **2020**, *13*, 2586.

[35] S. Laurent, L. vander Elst, R. N. Muller, *Contrast Media Mol. Imaging* **2006**, *1*, 128.

[36] N. Lewinski, V. Colvin, R. Drezek, *Small* **2008**, *4*, 26.

[37] P. Gurnani, C. Sanchez-Cano, H. Xandri-Monje, J. Zhang, S. H. Ellacott, E. D. H. Mansfield, M. Hartlieb, R. Dallmann, S. Perrier, *Small* **2022**, *18*, 2203070.

[38] M. Yu, J. Zheng, *ACS Nano* **2015**, *9*, 6655.

[39] H. Soo Choi, W. Liu, P. Misra, E. Tanaka, J. P. Zimmer, B. Itty Ipe, M. G. Bawendi, J. V. Frangioni, *Nat. Biotechnol.* **2007**, *25*, 1165.